metals

MDPI

Article

Transformation of Iron (III) Nitrate from an Aerosol by Ultrasonic Spray Pyrolysis and Hydrogen Reduction

Srecko Stopic [1,*], Ayadjenou Humphrey Hounsinou [1], Koffi Aka Stéphane [2], Tatjana Volkov Husovic [3], Elif Emil-Kaya [4] and Bernd Friedrich [1]

[1] IME Process Metallurgy and Metal Recycling, RWTH Aachen University, 52056 Aachen, Germany; humphrey.hounsinou@rwth-aachen.de (A.H.H.); bfriedrich@ime-aachen.de (B.F.)
[2] Training and Research Unit for Structure Sciences of Matter and Technology, University Felix Houphouet-Boigny, Cocody, Abidjan 00225, Côte d'Ivoire; xastinaka@gmail.com
[3] Faculty of Technology and Metallurgy, University of Belgrade, 11000 Belgrade, Serbia; tatjana@tmf.bg.ac.rs
[4] Department of Materials Science and Engineering, Norwegian University of Science and Technology, 7034 Trondheim, Norway; elif.e.kaya@ntnu.no
* Correspondence: sstopic@ime-aachen.de; Tel.: +49-241-80-95860

Abstract: Due to their unique properties, iron nanoparticles find diverse applications across various fields, including catalysis, electronics, wastewater treatment, and energy storage. Nano-iron particles are mostly sub-micrometer particles that are highly reactive to both air (oxygen) and water, and in nanoparticles (size below 100 nm), it is even more rapid than the bulk material. This characteristic limits its use in inert environments. Iron nanoparticles are not toxic and are mostly used for wastewater treatment. Understanding the hydrogen reduction mechanisms and conditions that lead to the formation of metallic iron particles from iron (III)-nitrate from an aerosol is crucial for enabling their effective utilization. In this work, we studied the hydrogen reduction behavior of Fe_2O_3 in the absence and presence of additives (SiO_2 or Pt). The particles were prepared via ultrasonic spray pyrolysis and hydrogen reduction. The characterization was performed with a scanning electron microscope, energy-dispersive X-ray spectroscopy, and X-ray diffraction. In the absence of additives, the oxygen content of iron oxide particles decreased with increasing temperature from 700 to 950 °C but significantly increased with the doping of 10 mL (40 wt.%) of SiO_2. The inhibitory effect of Si on the hydrogen reduction of Fe_2O_3 formed was more pronounced at 950 °C than at 700 °C. In contrast, the doping of only 5 mL (15 wt.%) of Pt significantly decreased the oxygen concentration in the synthesized particles by catalyzing the reduction reaction of iron oxides at 700 °C. The metallic iron (Fe) product, obtained in the undoped iron oxides run at only 950 °C, was also formed at 700 °C in the Pt-doped Fe_2O_3 run.

Keywords: iron; hydrogen reduction; ultrasonic spray pyrolysis

Citation: Stopic, S.; Hounsinou, A.H.; Stéphane, K.A.; Husovic, T.V.; Emil-Kaya, E.; Friedrich, B. Transformation of Iron (III) Nitrate from an Aerosol by Ultrasonic Spray Pyrolysis and Hydrogen Reduction. *Metals* **2023**, *13*, 1686. https://doi.org/10.3390/met13101686

Academic Editor: Daniel Assumpcao Bertuol

Received: 31 August 2023
Revised: 19 September 2023
Accepted: 25 September 2023
Published: 2 October 2023

1. Introduction

Efforts to reduce the substantial amount of CO_2 emissions in the iron industry often focus on developing more sustainable and advanced technologies. Among these techniques, ultrasonic spray pyrolysis (USP) has been recognized as a very simple, cost-effective, and highly efficient method for synthesizing uniform iron particles with finite and controlled sizes [1–3]. In the USP technique, a precursor solution is coldly atomized in a nebulizer, generating aerosol using ultrasound waves. Aerosol droplets are transported into a heating zone with a carrier gas, mainly a reducing agent, where they undergo evaporation, shrinkage, thermal decomposition, and densification to form spherical particles [4,5]. Besides the USP technique itself, choosing a preferable and environmentally friendly

reducing agent, like hydrogen, is another important step to further reduce massive CO_2 emissions in the iron industry.

However, previous studies showed that reducing hematite (Fe_2O_3), resulting from the thermal decomposition of an iron salt precursor solution, to metallic iron involves a sequence of steps that can go through intermediate phases, including magnetite (Fe_3O_4) and wüstite (FeO) as mentioned by Avalo et al. [6]. They assessed the thermodynamic feasibility of using hydrogen to reduce Fe_2O_3 by calculating the equilibrium mole fraction of H2 at different temperatures. At lower temperatures (~below 600 °C), the reduction of Fe_2O_3 by hydrogen is less thermodynamically favorable, and the reaction rate might be relatively slow. The primary product under these conditions is likely to be Fe_3O_4, with water as a by-product. In the intermediate temperature range of ~600–800 °C, the thermodynamic favorability of the reduction process increases. The main product becomes FeO. The extent of reduction to metallic iron becomes more substantial compared to lower temperatures. At elevated temperatures (~ 800–1200 °C), the reduction in Fe_2O_3 by hydrogen becomes highly thermodynamically favorable. The primary product is almost exclusively metallic iron (Fe). Water continues to be released as a by-product of the reaction. The reduction reaction processes are described in the following Equations (1)–(3):

$$3Fe_2O_3 + H_2(g) \rightarrow 2Fe_3O_4 + H_2O(g) \quad (1)$$

$$Fe_3O_4 + H_2(g) \rightarrow 3FeO + H_2O(g) \quad (2)$$

$$FeO + H_2(g) \rightarrow Fe + H_2O(g) \quad (3)$$

Our aim is to study the reduction in iron (III) nitrate using ultrasonic spray pyrolysis and the influence of additives such as silicon and platinum, which is missing in the literature.

$$2\ Fe(NO_3)_3 + 3\ H_2 \rightarrow 2\ Fe + 6\ HNO_3 \quad (4)$$

In a recent study, the effect of silicon (Si) on the hydrogen-based direct reduction in Fe_2O_3 at 700 °C was investigated via thin-film sputter deposition [7]. The authors found that the doping of a relatively low amount of Si (e.g., 3.7 at.%) significantly inhibited the hydrogen reduction process of Fe_2O_3 at 700 °C due to the creation of a layer enriched with SiOx on the surface of Si-doped Fe_2O_3.

On the other hand, researchers have also demonstrated how the hydrogen reduction (HR) of iron oxide can be accelerated using platinum (Pt). Platinum is a highly effective catalyst that provides an alternative reaction pathway with lower activation energy, enabling reactions to occur more readily and at lower temperatures [8]. In contrast to silicon, which blocks iron oxide-free surfaces, platinum provides active sites on its surface where hydrogen molecules can adsorb, dissociate into atomic hydrogen species, and react more readily with the iron oxide [9–11]. This mechanism, known as the hydrogen spillover effect, facilitates the breaking of chemical bonds within the iron oxide, promotes the reduction reaction, reduces the activation energy, and lowers the temperature at which hydrogen reduction takes place [12,13].

Although a lot of work has been done on the preparation of Fe-Si and Fe-Pt nanoparticles (NPs), there are only a few reports studying the effects of Si and Pt on the hydrogen-based direct reduction in Fe_2O_3, particularly via ultrasonic spray pyrolysis (USP). Therefore, the objective of this study is to investigate the hydrogen reduction behavior of Fe_2O_3 in the absence and presence of additives (SiO_2 or Pt). Specifically, the objectives of this work consist of using scanning electron microscopy (SEM), energy dispersive X-ray spectroscopy (EDS), and X-ray diffraction (XRD) analyses to (1) study the effect of the reaction temperature on the hydrogen-based reduction in Fe_2O_3 at 700 and 950 °C; (2) verify whether it is possible to inhibit the hydrogen reduction in Fe_2O_3 with silicon at 700 °C using a USP technique; (4) compare the effect of Si on the hydrogen-based reduction in

Fe_2O_3 at 700 and 950 °C; and study the effect of Pt on the hydrogen-based reduction in Fe_2O_3 at 700 °C using a USP technique.

2. Material and Methods

Iron nitrate nonahydrate [$Fe(NO_3)_3 \cdot 9H_2O$], 40 wt. % colloidal silica (SiO_2), and platinum nitrate solution ($N_4O_{12}Pt$, 15 wt. % of Pt) were used as the reagents. All the chemicals were purchased from Sigma-Aldrich company and used as received without further purification because of their analytical grade (≥99% pure).

Three precursor solutions of the same concentration (0.5 mol/L) and volume (400 mL) were prepared by dissolving 80.8 g of iron nitrate in deionized water and stirring for 30 min using a magnetic stirrer. Two of the solutions were mixed with 10 mL of SiO2 (40 wt. %) and 5 mL of Pt (15 wt. %), respectively, while the third one was left undoped.

The hydrogen reduction-assisted ultrasonic spray pyrolysis method was used to synthesize undoped Fe_2O_3, Si-doped Fe_2O_3, and Pt-doped Fe_2O_3 NPs. The setup consisted of hydrogen and argon gas bottles, a rotameter (Yokogawa Deutschland GmbH, Ratingen, Germany), a thermostat (JULABO, Seelbach, Germany), an ultrasonic atomizer PRIZNANO, PRIZMA; Kragujevac, Serbia (with three transducers) connected to a frequency generator, a silica glass tube heated using two combined furnaces (THERMOSTAR, Aachen, Germany), two wash bottles with deionized water for nanoparticle collection, and a gas exhaust pipe. The schematic view of the apparatus is shown in Figure 1.

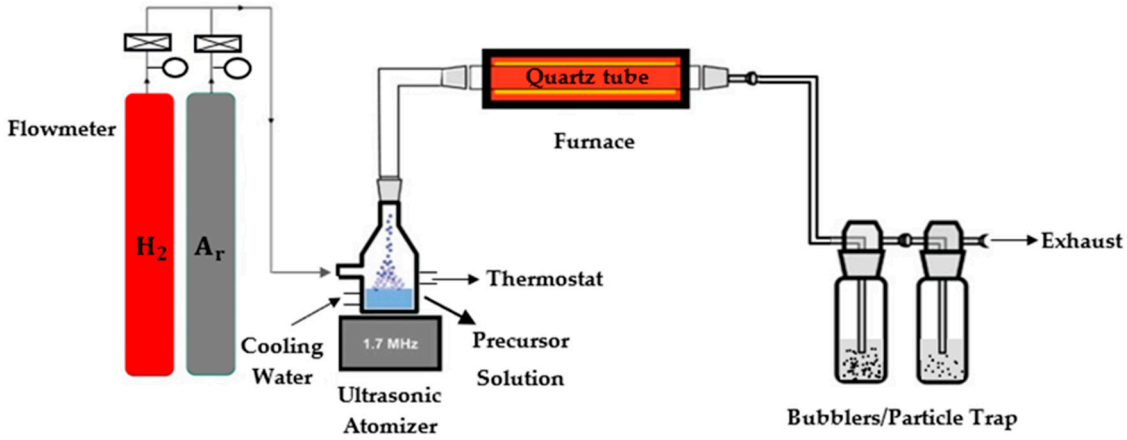

Figure 1. Schematic view of the USP-HR apparatus used for the synthesis of undoped iron oxides, Si-doped iron oxides, and Pt-doped iron oxides particles.

The USP-HR runs began with setting the furnace temperature, followed by loading the precursor solution through a funnel to a certain level of the atomizer. The solution was then nebulized at a frequency of 1.7 MHz into aerosol droplets under a gas flow rate of 3 L/min. To prevent the transducers from being damaged, the nebulizer temperature was controlled and cooled each time to 23 °C with water from the thermostat. The droplets were transported by the gas mixture into the horizontal tubular reactor. Hydrogen was especially used as a reducing agent at 2 L/min gas flow rate but also carried some of the droplets into the reactor. Argon with 1 L/min flow rate was used to maximize the transport of the aerosol droplets into the reactor. For safety reasons, argon was also used, before and after each experiment, to flush the quartz tube inside the furnaces to create an inert atmosphere conducive to the use of hydrogen.

Water evaporation, decomposition, and densification of droplets happened consecutively in the quartz tube heated by the electrical furnaces to form the nanoparticles. The total length of the silica tube is 83 cm with an inner diameter of 2.35 cm. Of this total length, 61 cm was heated by the furnaces, and 11 cm at each end of the tube was unheated.

Knowing the gas flow rate (3 L/min) and the geometry of the tubular reactor, the residence time was determined using the following Equation (5):

$$t = V_{tube}/q = \pi \cdot r^2 \cdot l/q \quad (5)$$

where q is the gas flow rate, r is the radius of the cylinder, l is the length of the glass tube heated by the furnace. The calculated T is ~5.3 s. So, the residence time for aerosol droplets passing through the heating zone of the tubular reactor was about 5.3 s.

After the completed reduction process, the obtained nanopowders were collected in the wash bottles connected to the outlet of the reactor, and the exhaust gases were vented to the outside atmosphere through a pipe. The operating time for each experiment was 2 h. The details of the experimental parameters for the synthesis of undoped iron oxides, Si-doped iron oxides, and Pt-doped iron oxides NPs are given in Table 1.

Table 1. Parameters used for the synthesis of Fe-alloy nanoparticles.

No.	Precursor Solution	Concentration (mol/L)	Temperature (°C)
1	Undoped iron oxides	0.5	700
2	Undoped iron oxides	0.5	950
3	Si-doped iron oxides	0.5	700
4	Si-doped iron oxides	0.5	950
5	Pt-doped iron oxides	0.5	700

At the end of each experiment, the obtained nanopowders (with deionized water) were removed from the wash bottles and placed in a large 2 L beaker to allow their sedimentation. Laboratory cleaning papers were used to cover the beaker to prevent contact of the NPs with air or oxygen. One day was enough for the complete sedimentation of the NPs. Afterward, the water was delicately removed from the beaker using a filter-based collection unit connected to a vacuum pump (Welch Ilmvac, Ilmenau, Germany). The nanoparticle suspension was collected in a small open glass bottle and dried in a vacuum oven at 100 °C to obtain powder samples for X-ray diffraction (XRD) analysis. The suspension was also sampled in a small bottle for scanning electron microscope (SEM) and energy disperse X-ray spectroscopy (EDS) analyses. SEM images were taken by Jeol JSM 7000F FEG-SEM, JEOL Ltd., Tokyo, Japan and used to observe the surface morphology of particles formed at different reaction parameters. The particle size and size distribution were investigated from SEM images using Image Pro Plus Software, Media Cybernetics, USA. EDX was carried out using Octane Plus by AMETEC Inc, Berwyn, PA, USA with a Si(Bi) X-ray detector connected to the SEM and a multi-channel analyzer to quantify the chemical composition of the particles. XRD analysis of powders was performed using a Bruker D8 Advance with a LynxEye detector (Bruker AXS, Karlsruhe, Germany). X-ray powder diffraction patterns were collected on a Bruker-AXS D4 Endeavor diffractometer in Bragg–Brentano geometry, equipped with a copper tube and a primary nickel filter providing Cu Kα1,2 radiation (λ = 1.54187 Å).

3. Results and Discussion

3.1. Influence of Temperature on HR of Undoped Fe_2O_3 NPs

Without the addition of additives, we expected the formation of the following products in the nanoparticles from the hydrogen reduction in Fe_2O_3 formed from iron (III) nitrate at 700 °C: magnetite (Fe_3O_4), wuestite (FeO) and possibly metallic iron (Fe). With an increase in temperature to 950 °C, FeO and Fe were anticipated to be formed.

SEM, EDS, and XRD images were used to investigate the effects of the temperature, ranging from 700 to 950 °C, on the microstructure and composition of undoped Fe_2O_3 particles at 0.5 mol/L. SEM images of iron oxide nanoparticles are given in Figure 2. Almost all particles had a spherical shape morphology with rough surfaces. Agglomeration of Fe_2O_3 NPs at 700 °C (Figure 2a) was reduced at 950 °C (Figure 2b) due to the formation of

large particles from the aggregates of small particles. Consequently, the boundaries between particles became more visible at 950 °C than at 700 °C. Moreover, it was observed that the diameters of the iron oxide particles were nearly unaffected by the variation of the reaction temperature (Figure 3). This is compatible with the work of Stopić et al. [14] on the synthesis of copper NPs, in which they reported that increasing the furnace temperature in the range of 800–900 °C had little or no effect in their experimental reactor.

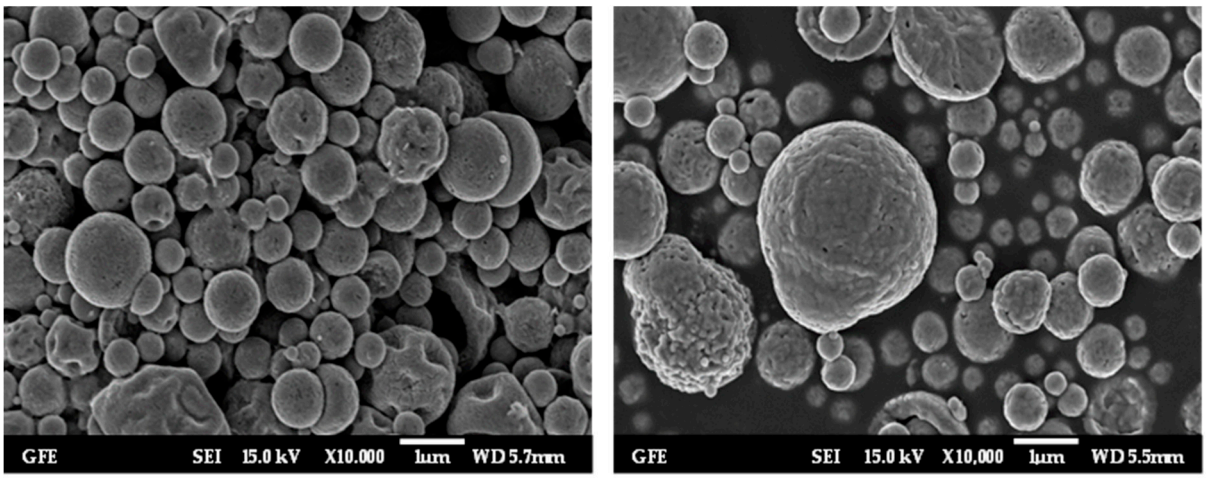

(**a**) (**b**)

Figure 2. SEM analysis of undoped iron oxide particles (**a**) 700 °C, (**b**) 950 °C.

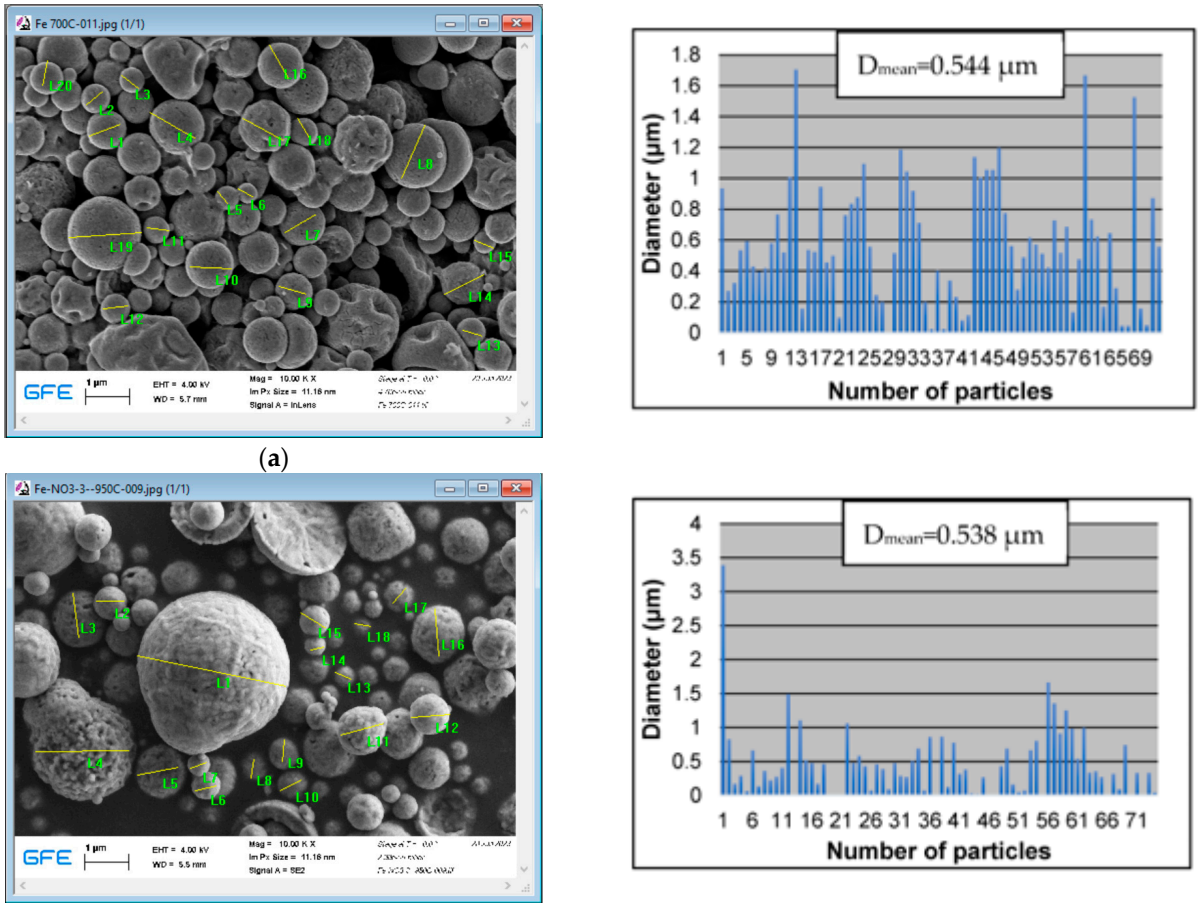

(**a**)

(**b**)

Figure 3. Mean diameters of undoped iron oxide particles (**a**) 700 °C, (**b**) 950 °C.

Although the maximum particle diameter jumped to 3.39 μm at 950 °C, the average particle size of undoped iron oxide nanoparticles slightly decreased from 544 to 538 nm with an increase in temperature from 700 to 950 °C, as demonstrated in Figure 2.

The theoretical particle size of undoped Fe_2O_3 NPs produced using the USP-HR method was determined by first determining the mean diameter of the aerosol droplet. The droplet and particle sizes are given using Equations (2) and (3), respectively:

$$D = 0.34(8 \cdot \pi \cdot \gamma/\rho \cdot f^2)^{1/3} \quad (6)$$

$$Dp = D(C_{precursor} \cdot M_{Fe}/M_{Fe(NO_3)_3 \cdot 9H_2O} \cdot \rho_{Fe})^{1/3} \quad (7)$$

where D is the average droplet diameter, γ is the surface tension of the solution, ϱ is the density of the solution, f is the frequency of the ultrasound, Dp is the particle diameter, Cprecursor is the solution concentration, Mproduct is the molar mass of iron, Msalt is the molar mass of $[Fe(NO_3)_3 \cdot 9H_2O]$, and $\rho_{product}$ is the density of iron.

Using Equation (2) and the parameters of the study (γ: $72.9 \cdot 10^{-3}$ Nm^{-1}; ρ: 1 g/cm^3; f: 1.7 MHz), the droplet diameter was calculated as 2.92 μm. Thus, the theoretical particle diameter for 0.5 M iron nitrate precursor solution, employing Equation (3), was calculated as 445 nm. The reason why the experimental particle sizes at 700 and 950 °C, 544 and 538 nm, respectively, were bigger than the theoretical one may be explained by the lower rate of aggregation [15] and sintering [16] of the particles due to less residence time of iron oxide droplets in the reaction zone at higher temperatures.

The quantitative results based on the EDS spectrums (Figure 4) of undoped Fe_2O_3 NPs are given in Table 2. EDS analysis indicates that particles produced from both reaction temperatures contained iron and a significant amount of oxygen. However, the atomic percentage of oxygen considerably decreased from 51.74% to 31.15% with an increase in temperature from 700 to 950 °C. When comparing the iron-to-oxygen (Fe/O) atomic ratios in the synthesized nanoparticles at different temperatures, we realized that the one at 950 °C (~100%) was greater than that at 700 °C (~ 93%) (Table 2). So, the increase in reaction temperature is necessary for the elimination of some traces of oxygen from the produced nanopowder [14].

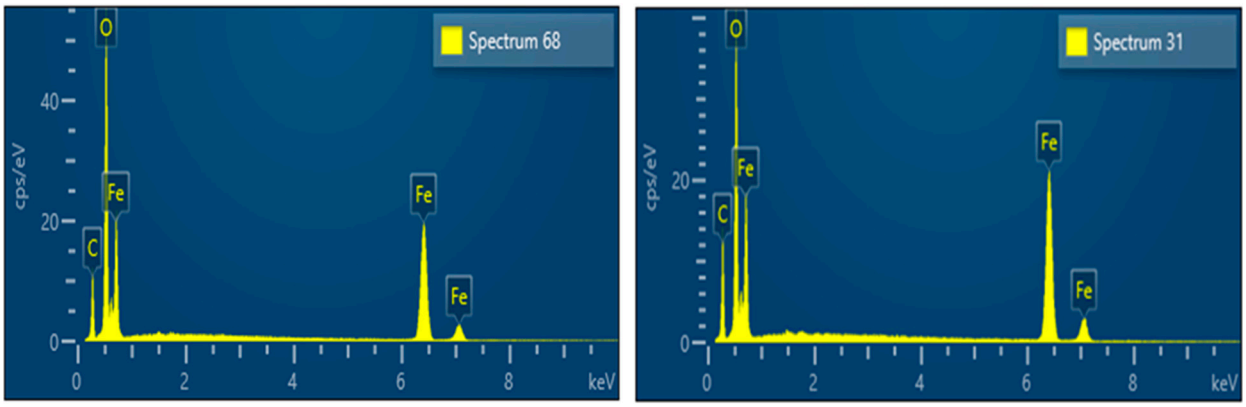

(**a**) (**b**)

Figure 4. EDS spectrums for iron oxide particles are produced at (**a**) 700 °C and (**b**) 950 °C.

Table 2. Atomic percentage of elements in Fe_2O_3 particles obtained using EDS analysis.

		It		T (950 °C)	
Element	**Atom. Mass (g/mol)**	**Weight (%)**	**Atom. (%)**	**Weight (%)**	**At. (%)**
Iron	55.845	76.5	48.26	65.4	31.89
Oxygen	16	23.5	51.74	18.3	31.15

Carbon	12.01	–	–	16.3	36.96

Although the atomic percentage of carbon is negligible in the synthesized particles at 700 °C, the EDS spectrum (Figure 4) shows that there was a small amount of carbon detected even though its peak is weak. Carbon peaks observed at 700 and 950 °C resulted from the use of the glassy carbon slide (substrate) to fabricate the thick film for SEM/EDS characterization. Moreover, EDS spectrums show that no impurities, such as nitrogen, were detected in the chemical composition of the particles.

All the obtained XRD patterns exhibited multiple peaks or diffraction angles (Figure 5), making it difficult to distinguish and identify individual phases or crystal structures. We believe that employing high-resolution and 2D-XRD techniques is necessary to achieve accurate phase identification. However, the patterns shown in Figure 5 suggest that the hydrogen reduction in Fe_2O_3 to Fe_3O_4 (as shown with Equation (1)) in the absence of additives was complete at both reaction temperatures, leaving no traces of hematite behind. They clearly reveal that the products formed at 700 °C were Fe_3O_4 and FeO (Figure 5), while those at 950 °C were Fe_3O_4, FeO, and Fe (Figure 5). Magnetite exhibited higher peaks in the synthesized particles at both reaction temperatures than the other products. Wuestite, resulting from the reduction in magnetite, was also present at both temperatures and was further reduced to iron with an increase in temperature from 700 to 950 °C (as shown in Equation (2)). However, the iron peak was lower compared to that of the other products at 950 °C. Thus, XRD and EDS results are compatible with each other.

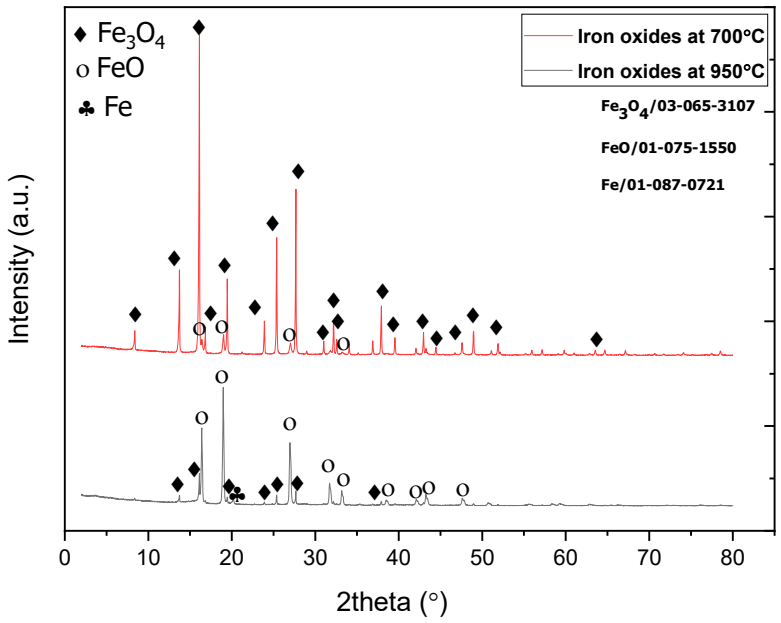

Figure 5. XRD patterns of iron oxide particles produced at 700 °C and 950 °C.

3.2. Influence of Silicon on HR of Fe_2O_3 NPs

By adding 10 mL of colloidal silica (40 wt.% SiO_2) to 400 mL of 0.5 M iron nitrate solution, we expected the hydrogen reduction in Fe_2O_3 to be inhibited, resulting in the formation of only Fe_3O_4, with some remaining traces of Fe_2O_3.

The effect of the Si content of the precursor mixture on the microstructure and size of iron trioxide nanoparticles was investigated using SEM. Comparative analysis of SEM images of undoped Fe_2O_3 NPs (Figure 2) versus those of Si-doped Fe_2O_3 NPs (Figure 6) suggests that the darker particle-like objects were iron particles and were caged by brighter siliceous materials. In the Si-doped Fe_2O_3 runs, spherical particles with smooth

surfaces were produced. At both temperatures, the agglomeration and formation of large particles were more pronounced than that of the Fe_2O_3-only experiments (Figure 6).

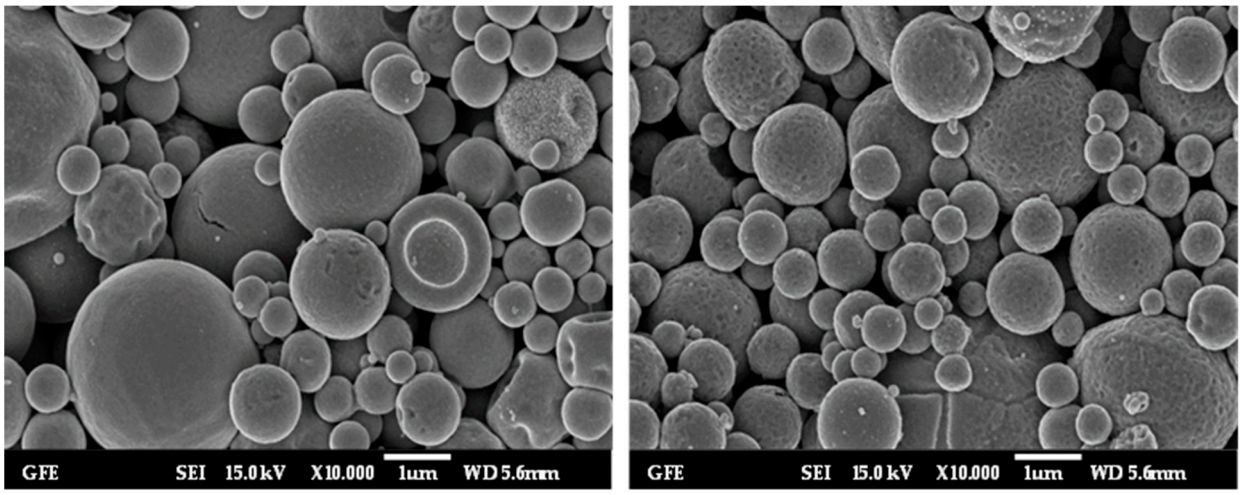

(**a**) (**b**)

Figure 6. SEM analysis of Si-doped iron oxide particles (**a**) 700 °C, (**b**) 950 °C.

The size distribution of Si-doped Fe_2O_3 NPs is shown in Figure 7. With the addition of a small quantity of SiO_2 to the iron nitrate solution, the average particle size significantly increased from 544 to 877 nm and from 538 to 1032 nm at 700 and 950 °C, respectively (Figures 3 and 7). The slight decrease in particle size observed in Fe_2O_3-only runs when the temperature increased to 950 °C was also inhibited by Si doping. These results confirm the previously mentioned results from Patterer et al. [7]. Their investigation revealed that the doping of 3.7 at.% Si significantly inhibits hydrogen direct reduction in Fe_2O_3 at 700 °C by forming a SiOx-enriched layer in the surface near-region. Additionally, we found that this inhibition is valid also at 950 °C.

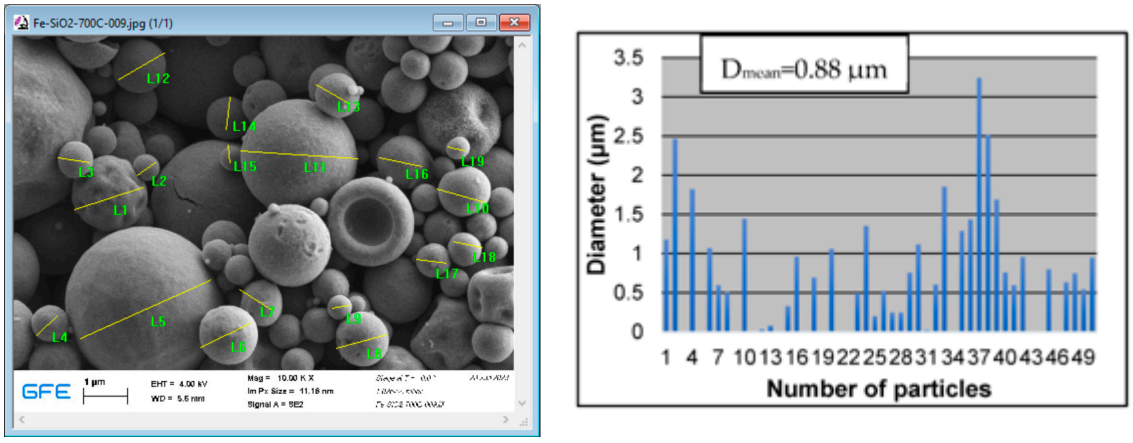

(**a**)

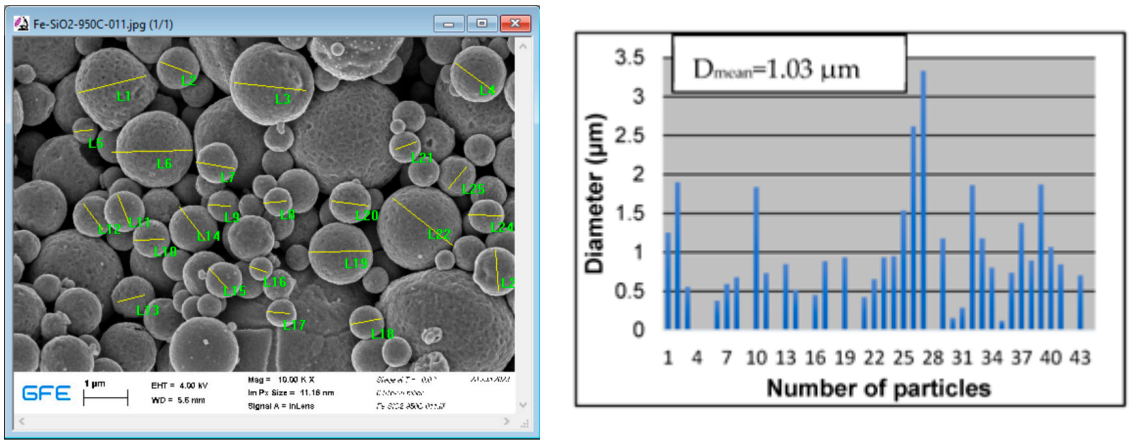

(**b**)

Figure 7. Mean diameters of Si-doped iron oxide particles (**a**) 700 °C, (**b**) 950 °C.

EDS analysis was used to clarify the chemical composition of the synthesized Fe-Si nanoparticles (Figure 8). The quantitative results from the two Fe-Si EDS spectra, presented in Table 3, indicate that when Si was included in the experiments, the atomic percentage of oxygen became slightly higher in the Si-doped Fe_2O_3 NPs compared to the undoped Fe_2O_3 NPs. However, the atomic percentage of iron drastically decreased to 19.91 or 18.40 at.% at 700 and 950 °C, respectively (Tables 2 and 3). This suggests that the reduction reaction of Fe_2O_3 in an Ar-H_2 atmosphere becomes less efficient when alloyed with Si in comparison to unalloyed Fe_2O_3. Furthermore, as the temperature increased to 950 °C, we noticed that the oxygen content in the Fe-Si nanoparticles increased slightly from 43.91 to 45.97 at.%, whereas the opposite was observed in the Fe_2O_3-only runs. Consequently, the atomic percentage of iron slightly decreased from 19.91 to 18.40 at.%, signifying that the temperature increase further inhibits the hydrogen reduction in iron oxide nanoparticles during Si doping.

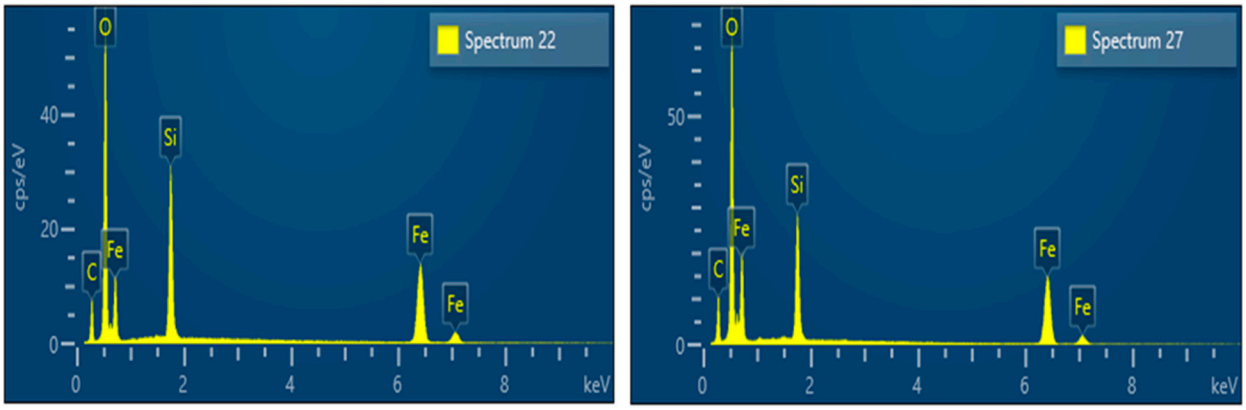

(**a**) (**b**)

Figure 8. EDS spectrums for Si-doped NPs produced at (**a**) 700 °C, (**b**) 950 °C.

Table 3. Atomic percentage of elements in iron oxides Si-doped Fe_2O_3 particles obtained using EDS analysis.

		T (700 °C)		T (950 °C)	
Element	**Atom. Mass (g/mol)**	**Weight (%)**	**Atom. (%)**	**Weight (%)**	**Atom. (%)**
Iron	55.845	46.1	19.91	44.3	18.40
Oxygen	16	29.1	43.91	31.7	45.97
Silicon	28.086	11.7	10.06	9.7	8.00
Carbon	12.01	13.1	26.12	14.3	27.63

XRD patterns of the Si-doped Fe_2O_3 runs reveal that the products formed at both reaction temperatures are Fe_3O_4, FeO, and Fe_2SiO_4 (Figure 9). No metallic iron (Fe) was formed at any temperature. This suggests that the hydrogen reduction in iron trioxide was not complete. Silicon acts on Fe_2O_3 by creating a layer enriched with SiOx on the surface of Si-doped Fe_2O_3 to block free surfaces of iron oxide, hindering their direct interactions with the hydrogen-reducing agent [7]. We also noticed that the peak of Fe_2SiO_4 in the synthesized particles at 950 °C was higher than that at 700 °C, which proves that Si doping further inhibits the hydrogen reduction in Fe_2O_3 at higher temperatures.

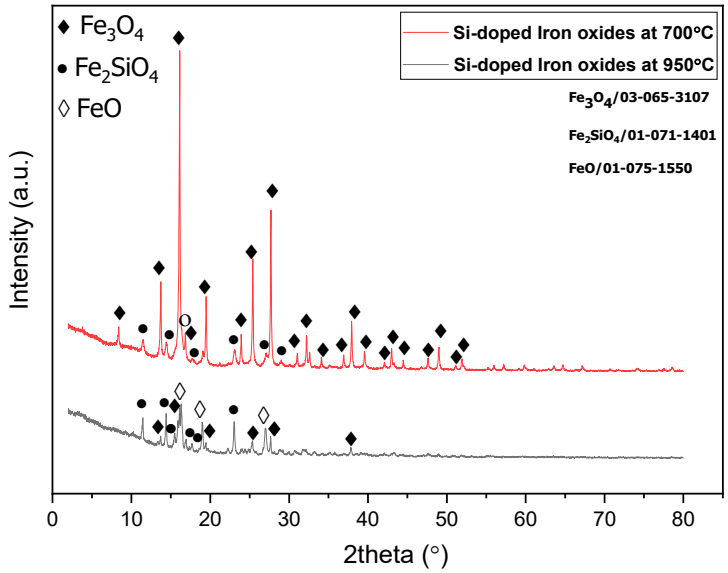

Figure 9. XRD patterns of Si-doped iron oxide particles at 700 °C and 950 °C.

3.3. Platinum Effect on HR of Fe_2O_3 NPs

Upon introducing 5ml of platinum (IV) nitrate solution (15 wt.% Pt) into 400 mL of 0.5 M iron nitrate solution, our expectation was that the hydrogen reduction in Fe_2O_3 would be accelerated, resulting in the formation of FeO and Fe, with no residual traces of Fe_2O_3.

SEM, EDS, and XRD analyses were also used to investigate the influence of platinum on the particle size and composition of iron trioxide nanoparticles at 700 °C. In the iron oxides-only experiments at 700 °C, long aggregates, consisting of primary particles with an average size of about 544 nm, were formed, and the boundaries between these particles were not clear (Figures 2a and 3a). With the addition of a very small quantity of Pt to the iron nitrate solution, the agglomeration of particles decreased significantly; the average particle size slightly increased to 0.59 µm, and the boundaries became clearer (Figures 10a and 11).

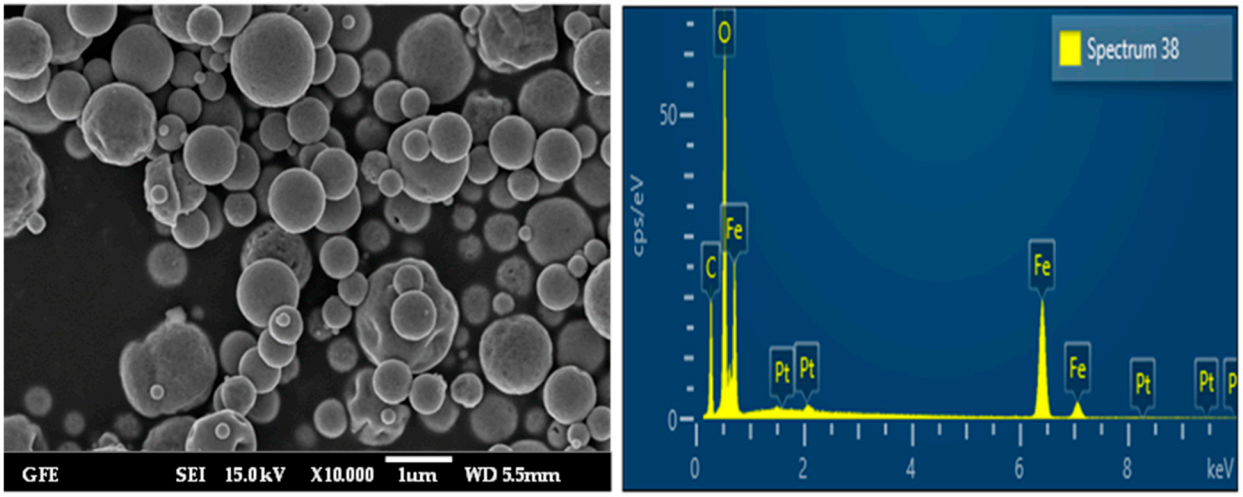

(**a**) (**b**)

Figure 10. Analysis of Fe-Pt NPs with (**a**) SEM and (**b**) EDS images at 700 °C.

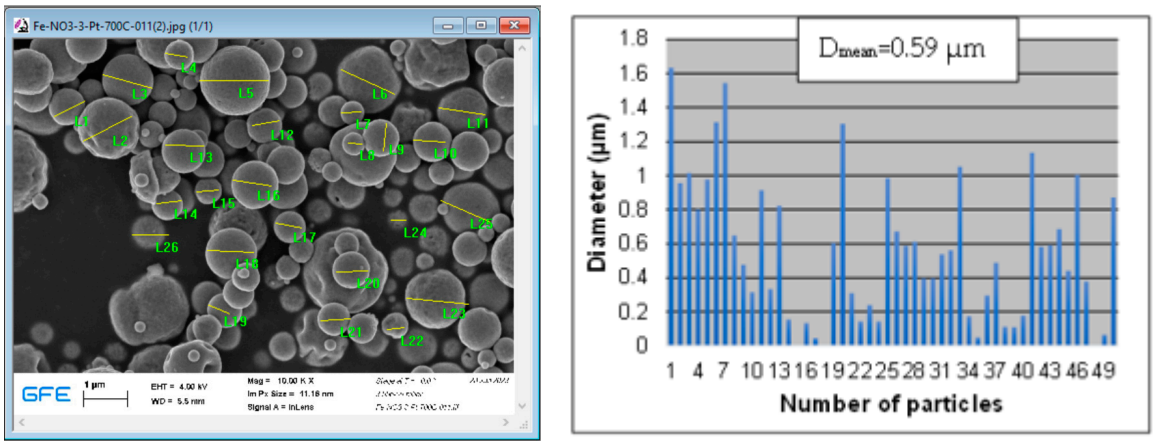

Figure 11. Mean diameter of Pt-doped iron oxide particles at 700 °C.

The quantitative results based on the EDS spectrums (Figure 10b) of Pt-doped iron oxide NPs at 700 °C are given in Table 4. EDS analysis indicates that when iron oxides were doped with Pt, the atomic percentage of oxygen experienced a significant decrease from 51.74 to 36.51 at.% after the hydrogen reduction treatment. However, the Fe/O atomic ratio in the synthesized Fe-Pt particles was slightly lower than that in the undoped iron oxide particles at 700 °C (Tables 2 and 4). Despite this observation being noted, the

XRD pattern suggests that, in addition to the Fe_3O_4 and FeO products, metallic iron (Fe) was formed during Pt doping at 700 °C (Figure 12). In the Fe_2O_3-only runs, Fe was only formed at the higher temperature of 950 °C. This implies that, even at low temperatures and with a relatively low concentration of Pt (0.09 at.%), Fe could be directly obtained from the hydrogen reduction in iron trioxide.

Table 4. Atomic percentage of elements in Pt-doped Fe_2O_3 particle obtained using EDS analysis.

Element	Atom. Mass (g/mol)	Weight (%)	At (%)
Iron	55.845	59.6	27
Oxygen	16	23.1	36.51
Platinum	195.084	0.7	0.09
Carbon	12.01	17.3	36.42

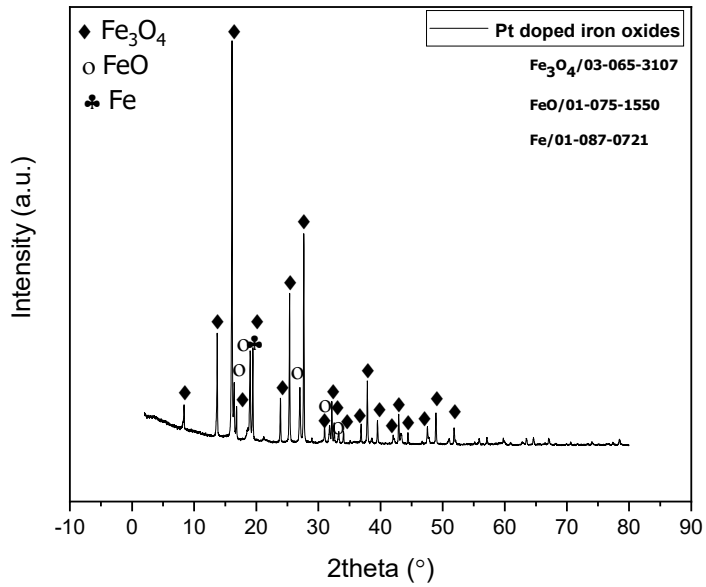

Figure 12. XRD patterns of Pt-doped iron oxides produced at 700 °C.

Unlike silicon, which blocks the free surfaces of iron oxide, platinum offers active sites on its surface to facilitate the adsorption of hydrogen molecules, their subsequent dissociation into atomic hydrogen species, and a more facile reaction with the iron oxide [10,11]. We believe that by increasing the platinum concentration in the precursor solution, the Fe/O atomic ratio in the synthesized Fe-Pt NPs would be greater than that in the undoped Fe_2O_3 NPs at 700 °C. By taking this aspect into consideration and performing calculations for the relative concentration or atomic percentage of iron and oxygen, based on Tables 2 and 3, a scenario like the one illustrated in Figure 13 can be anticipated:

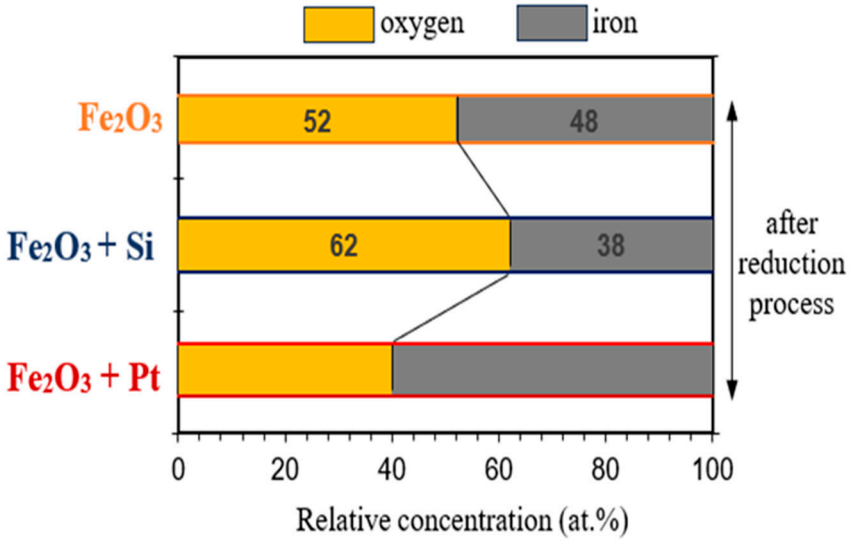

Figure 13. The oxygen-to-iron atomic ratio of undoped, Si-doped, and Pt-doped iron oxide nanoparticles after hydrogen reduction at 700 °C.

Liu et al. [17] mentioned that in physical mixtures of platinum-containing mordenite with Fe_2O_3, no enhancement of the Fe_2O_3 reduction is found if the Pt is present as Pt^0 inside the zeolite, but a very strong enhancement is observed if an oxidative pretreatment enables the Pt to migrate, as an oxide or as Pt ions, out of the zeolite onto the iron oxide. Although we did not detect it, we suppose that the spillover effect is enabled by platinum ions in ultrasonic spray pyrolysis with hydrogen reduction.

4. Conclusions

The hydrogen reduction-assisted ultrasonic spray pyrolysis (USP-HR) technique was used to successfully produce undoped iron oxides, Si-doped iron oxides, and Pt-doped iron oxide particles at 700 and 950 °C. The primary focus of this study was to investigate the hydrogen reduction behavior of iron trioxide (Fe_2O_3) in the absence and presence of additives (SiO_2 or Pt). The investigation revealed that the oxygen content of iron oxide particles, in the absence of additives, decreases with increasing temperature from 700 to 950 °C but significantly increases with the doping of 10 mL (40 wt.%) of SiO_2 at both reaction temperatures. The introduction of Si into the precursor solution inhibits the hydrogen reduction in Fe_2O_3 by creating a layer enriched with SiOx on the surface of Si-doped Fe_2O_3 to block free surfaces of iron oxide, hindering their direct interactions with the reducing agent. The reduction inhibition, in the presence of Si, becomes even more pronounced at higher temperatures (950 °C). In contrast, the doping of only 5 mL (15 wt.%) of Pt significantly decreased the oxygen concentration in the synthesized particles by accelerating the hydrogen reduction in Fe_2O_3 at 700 °C. Metallic iron (Fe), obtained in the undoped Fe_2O_3 run at only 950 °C, was also formed at 700 °C in the Pt-doped iron oxides run. At low temperatures and with a low Pt concentration, Fe particles can be produced directly from the hydrogen reduction in Fe_2O_3 due to platinum's catalytic role in offering active sites on its surface to induce a hydrogen spillover effect.

It is shown that catalytic reactions often involve the manipulation of surface oxygen species, and the knowledge gained from this study could lead to improved catalyst design and performance. The ability to efficiently generate metallic iron (Fe) from iron oxide nanoparticles at lower temperatures, especially with Pt doping, could enhance catalytic activity in hydrogenation processes. Si-doped iron oxide NPs could also be used to create catalyst supports with enhanced stability and controlled redox properties.

Author Contributions: Conceptualization, A.H.H. and S.S.; methodology, S.S.; software, E.E.-K.; validation, A.H.H. and E.E.-K.; formal analysis, T.V.H.; investigation, A.H.H.; resources, S.S.; data curation, A.H.H.; writing—original draft preparation, A.H.H., S.S., K.A.S., B.F., E.E.-K. and T.V.H.; writing—review and editing, S.S.; visualization, T.V.H.; supervision, S.S., K.A.S. and B.F.; project administration, S.S.; funding acquisition, B.F. and K.A.S. All authors have read and agreed to the published version of the manuscript.

Funding: This research was funded by the Federal Ministry of Education and Research, Germany, grant number 03SF0626C. The APC was funded by MDPI, Basel, Switzerland.

Institutional Review Board Statement: Not applicable.

Informed Consent Statement: Not applicable.

Data Availability Statement: Not applicable.

Conflicts of Interest: The authors declare no conflict of interest.

References

1. Jelen, Ž.; Majeric, P.; Zadravec, M.; Anžel, I.; Rakuša, M.; Rudolf, R. Study of gold nanoparticles' preparation through ultrasonic spray pyrolysis and lyophilisation for possible use as markers in LFIA tests. *Nanotechnol. Rev.* **2021**, *10*, 1978–1992.
2. Toparli, C.; Ebin, B.; Gürmen, S. Synthesis, structural and magnetic characterization of soft magnetic nanocrystalline ternary FeNiCo particles. *J. Magn. Magn. Mater.* **2017**, *423*, 133–139. https://doi.org/10.1016/j.jmmm.2016.09.005.
3. Majeric, P.; Rudolf, R. Advances in ultrasonic spray pyrolysis processing of noble metal nanoparticles-Review. *Materials* **2020**, *13*, 3485.
4. Ebin, B.; Gürmen, S. Synthesis and Characterization of Nickel Particles by Hydrogen Reduction Assisted Ultrasonic Spray Pyrolysis(USP-HR) Method. *KONA Powder Part. J.* **2011**, *29*, 134–140. https://doi.org/10.14356/kona.2011016.
5. Toparli, C.; Ebin, B.; Gürmen, S. Iron-Nickel-Cobalt (Fe-Ni-Co) Alloy Particles Prepared by Ultrasonic Spray Pyrolysis and Hydrogen Reduction (USP-HR) Method. In *Processing and Properties of Advanced Ceramics and Composites V*; John Wiley & Sons, Ltd.: Hoboken, NJ, USA, 2013; pp. 247–254. https://doi.org/10.1002/9781118744109.ch27.
6. Avalo, O.; Moura, F.; Brocchi, E.; Navarro, R.C.s. Synthesis of Fe-Ni alloys by reduction with hydrogen. In Proceedings of the 65th ABM International Congress, 18th IFHTSE Congress and 1st TMS/ABM International Materials Congress, Rio de Janeiro, Brazil, 26–30 July 2010; Volume 3, pp. 2277–2289.
7. Patterer, L.; Mayer, E.B.; Mráz, S.; Pöllmann, P.J.; Hans, M.; Primetzhofer, D.; Souza Filho, I.R.; Springer, H.J.; Schneider, J.M. Effect of Si on the hydrogen-based direct reduction of Fe2O3 studied by XPS of sputter-deposited thin-film model systems. *Scr. Mater.* **2023**, *233*, 115515. https://doi.org/10.1016/j.scriptamat.2023.115515.
8. Miller, J.T.; Meyers, B.L.; Barr, M.K.; Modica, F.S.; Koningsberger, D.C. Hydrogen Temperature-Programmed Desorptions in PlatinumCatalysts: Decomposition and Isotopic Exchange by Spillover Hydrogen of Chemisorbed Ammonia. *J. Catal.* **1996**, *159*, 41–49. https://doi.org/10.1006/jcat.1996.0062.
9. Spreafico, C.; Karim, W.; Ekinci, Y.; van Bokhoven, J.A.; VandeVondele, J. Hydrogen Adsorption on Nanosized Platinum and Dynamics of Spillover onto Alumina and Titania. *J. Phys. Chem. C* **2017**, *121*, 17862–17872. https://doi.org/10.1021/acs.jpcc.7b03733.
10. Karim, W.; Spreafico, C.; Kleibert, A.; Gobrecht, J.; VandeVondele, J.; Ekinci, Y.; van Bokhoven, J.A. Catalyst support effects on hydrogen spillover. *Nature* **2017**, *541*, 68–71. https://doi.org/10.1038/nature20782.
11. Meng, Z.; Xiao, F.; Wei, Z.; Guo, X.; Zhu, Y.; Liu, Y.; Li, G.; Yu, Z.-Q.; Shao, M.; Wong, W.-Y. Direct synthesis of L10-FePt nanoparticles from single-source bimetallic complex and their electrocatalytic applications in oxygen reduction and hydrogen evolution reactions. *Nano Res.* **2019**, *12*, 2954–2959. https://doi.org/10.1007/s12274-019-2537-y.
12. Lin, S.-D.; Vannice, M.A. Toluene Hydrogenation Over Supported Platinum Catalysts. In *Studies in Surface Science and Catalysis*; Guczi, L., Solymosi, F., Tétényi, P., Eds.; Elsevier: Amsterdam, The Netherlands, 1993; Volume 75, pp. 861–874. https://doi.org/10.1016/S0167-299164062-8.
13. Rioux, R.M.; Song, H.; Hoefelmeyer, J.D.; Yang, P.; Somorjai, G.A. High-Surface-Area Catalyst Design: Synthesis, Characterization, and Reaction Studies of Platinum Nanoparticles in Mesoporous SBA-15 Silica. *J. Phys. Chem. B* **2005**, *109*, 2192–2202. https://doi.org/10.1021/jp048867x.
14. Stopic, S.; Friedrich, B.; Volkov Husovic, T.; Vuksanovic, M. Characterisation of nano-powder morphology obtained by ultrasonic spray pyrolysis. *J. Metall.* **2008**, *14*, 41–54.
15. Okuyama, K.; Kousaka, Y.; Tohge, N.; Yamamoto, S.; Wu, J.J.; Flagan, R.C.; Seinfeld, J.H. Production of ultrafine metal oxide aerosol particles by thermal decomposition of metal alkoxide vapors. *AIChE J.* **1986**, *32*, 2010–2019. https://doi.org/10.1002/aic.690321211.
16. Jang, H.D.; Jeong, J. The Effects of Temperature on Particle Size in the Gas-Phase Production of TiO_2. *Aerosol Sci. Technol.* **1995**, *23*, 553–560. https://doi.org/10.1080/02786829508965337.
17. Liu, H.-Y.; Chiou, W.A.; Frohlic, G.; Sachtler, W. Platinum migration out of zeolites onto iron oxide: An alternative to H spillover. *Top. Catal.* **2000**, *10*, 49–57.